Revue des Composites et des Matériaux Avancés-Journal of Composite and Advanced Materials
Vol. 36, No. 1, February, 2026, pp. 89-95
Journal homepage: http://iieta.org/journals/rcma

Laser Selective Welding of Metal Powder Creates Spatial Lattice Structures in Channels (Part 2)

Enaam Obeid Hassoun[1], Hussain Abdulaziz Abrahem[1*], Alexey A. Lopatin[2], Rozaliya A. Gabdullina[2], A. A. Saetgaraev[2], A. R. Biktagirova[2], Aleksandr A. Terentev[3]

[1] Department of Electromechanical Engineering, University of Technology, Baghdad 10066, Iraq
[2] Department of Jet Engines and Power Plants, Federal State Budgetary Educational Institution of Higher Education «Kazan National Research Technical University named after A.N. Tupolev–KAI», Kazan 420111, Russian Federation
[3] Department of Laser and Additive Technologies, Federal State Budgetary Educational Institution of Higher Education «Kazan National Research Technical University named after A.N. Tupolev–KAI», Kazan 420111, Russian Federation

Corresponding Author Email: Hussain.A.Abrahem@uotechnology.edu.iq

https://doi.org/10.18280/rcma.360109

Received: 25 September 2025
Revised: 30 November 2025
Accepted: 17 February 2026
Available online: 28 February 2026

Keywords:
lattice structure, spatial lattice radiator, heat transfer intensification

ABSTRACT

This study investigates the hydraulic performance of channels integrated with spatially ordered lattice structures fabricated by Selective Laser Melting (SLM). While lattice structures are recognized for their superior strength-to-weight ratio, their controlled application for optimizing fluid flow and heat transfer in thermal management systems remains underexplored. We focus on the experimental and numerical analysis of pressure drop and hydraulic resistance in channels with two distinct lattice densities, comparing them against a smooth channel. A key aspect of our investigation is the analysis of the discrepancy between experimental data and numerical simulations using the k-ε turbulence model, which we attribute to the significant surface roughness inherent in the SLM process. Our findings demonstrate that lattice structures, despite increasing hydraulic resistance, offer a vast surface area for heat exchange, making them promising for compact heat exchangers under high thermal loads. This work provides quantitative data and critical insights into the design trade-offs and modeling challenges for SLM-fabricated lattice heat sinks.

1. INTRODUCTION

The escalating thermal loads in modern radio-electronic and electrical power equipment necessitate the development of advanced cooling solutions that combine high heat transfer efficiency with structural integrity [1-3]. Within this context, porous heats (PHEs) have long been considered promising due to their ability to significantly increase the effective heat transfer area within a constrained volume [4, 5]. Traditionally, PHEs with disordered, chaotic porosity (e.g., metal foams) have been utilized, capitalizing on their large specific surface area for high heat exchange intensity. However, their inherent limitations—including unpredictable flow paths, dead-end pores, and consequently high hydraulic resistance—often restrict their application to short segments under extreme thermal loads [6]. The compromise between thermal efficiency and pressure reduction constitutes a fundamental difficulty in thermal management design.

A paradigm shift is offered by spatially ordered lattice structures, fabricated additively [7-9]. These architectures provide the coveted high surface-area-to-volume ratio of porous materials while enabling deliberate control over the flow path, thereby eliminating dead-end pores and reducing hydraulic resistance compared to their stochastic counterparts [1, 4, 10]. Furthermore, their controlled anisotropy allows for the design of load-bearing components with integrated cooling functionality, maximizing material efficiency [1, 11, 12]. The advent of Selective Laser Melting (SLM) has made the fabrication of such complex, tailored geometries economically viable for high-value applications, from aerospace to advanced electronics [3, 4, 11].

While the mechanical properties of strut-based lattice structures have been extensively studied [1, 4], their fluid flow and thermal-hydraulic characteristics remain a critical and less explored research frontier [13, 14]. Current literature often relies on numerical simulations that idealize the SLM process, modeling lattice struts with perfectly smooth surfaces [13, 15]. However, the reality of SLM fabrication involves significant surface roughness and micro-scale morphological deviations from the digital model, as shown in Figure 1, which are known to profoundly impact flow resistance and heat transfer [3, 11]. This creates a critical gap between predictive models and real-world performance, hindering the reliable design of lattice-based heat exchangers [16, 17].

The promising application of spatially lattice-based radiators in cooling and thermal stability systems has become a topic that must be researched and explained in various ways to highlight its importance to a wider range of researchers from

around the world [18, 19]. Progress was demonstrated by fabricating TPMS-based Gyroid and Diamond structures with new density, heterogeneous structure, and cell size gradients from Ti-6Al-4V via SLM, resulting in a unique gradient pore size variation as in the study [20].

Therefore, this study bridges this gap by presenting a coupled experimental and numerical investigation of the hydraulic performance of SLM-fabricated spatial lattice structures integrated into cooling channels. We focus specifically on quantifying the pressure drop and hydraulic resistance for two distinct lattice densities and comparing them against a baseline smooth channel. A central aim is to critically evaluate the predictive capability of a standard k-ε turbulence model when confronted with the inherent surface roughness of as-built SLM components. By elucidating the causes of the discrepancy between simulation and experiment, this work provides indispensable insights and quantitative data for the future design and accurate modeling of high-performance, additively manufactured heat exchange systems.

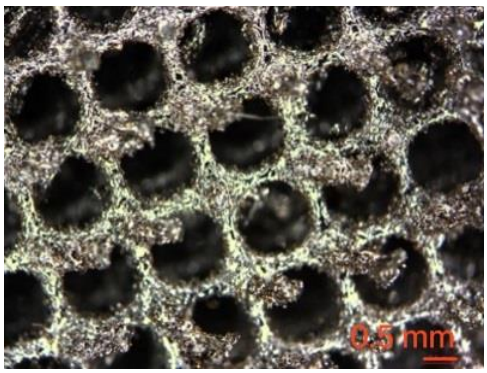

(a) At scale 0.5 mm

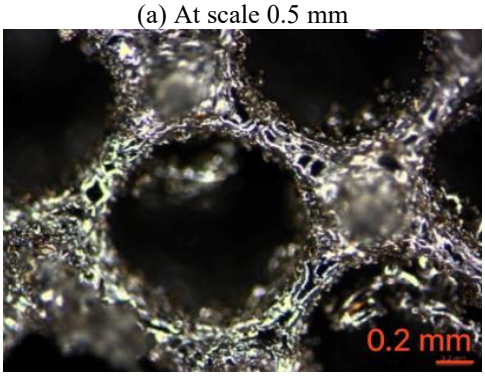

(b) At scale 0.2 mm

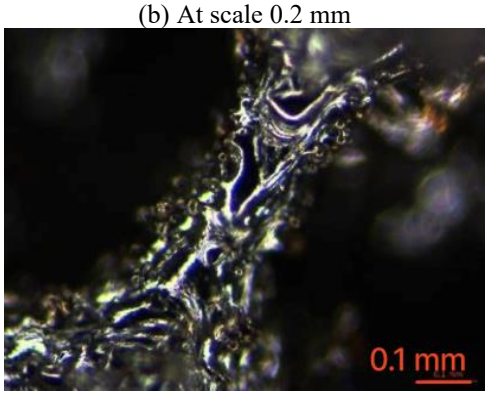

(c) At scale 0.1 mm

Figure 1. Scanning Electron Microscope (SEM) images of the Selective Laser Melting (SLM)-fabricated spatial lattice structure (Working Area No. 3) at different magnifications

Note: showing (a) the overall periodic structure at 0.5 mm scale, and (b, c) the characteristic surface roughness and partially sintered powder particles at higher magnifications (0.2 mm and 0.1 mm scales, respectively).

2. MATERIALS AND METHODS

2.1 Method for manufacturing spatial lattice structures

Selective laser sintering is used to create spatial lattice structures. The mean pore diameter ranged from 1.2 mm with a standard deviation of 25 μm. A 3D printed section was produced using a laser selective sintering machine (EOSINT M270) to create finished metal powder products as well as prototypes. While operating the installation and using a specialized feeding mechanism, the powder is added to either the prior layer or to the surface of the working platform. The layer is smoothed at the same time as the substance is applied. The used powder was pH 1 with a granulation of 20-40 mkm. The chemical composition of the powder used is given in Table 1.

Table 1. Composition of the chemical powder [21]

Element	Min.	Max.
Cr	14	15.5
Ni	3.5	5.5
Cu	2.5	4.5
Mn	-	1
Si	-	1
C	-	0.07
Mo	-	0.5
Nb	0.15	0.45

Layer thickness shifts based on the establishment specifics and the fabric utilized, extending from 0.015 mm to 0.15 mm. Another, the laser specifically wires the ranges of the layer that are included within the object, whereas combining them with the past one. Following the consequent sintering, the stage is diminished in order to coordinate layer thickness. An additional powder layer is managed, and the cycle is performed once more. Surface roughness of the working parts was measured using a model 130 profilometer, specifically intended for determining profile parameters and roughness. The typical roughness is Ra 20 mkm. The measurements were conducted using the center line system, following the guidelines outlined in GOST 25142-82. The measuring instrument is classified as a first-class accuracy device. The inductive sensor of the profilometer has a sensitivity of 0.002 microns, allowing it to accurately measure surface imperfections with a height of 0.005 microns. Figure 1 shows the spatial lattice of working area No. 3 magnified at various magnifications.

These images are original and unmodified, illustrating the surface morphology that influences hydraulic performance.

2.2 Numerical model and boundary conditions

Numerical modeling represents a highly effective methodology for analyzing the hydraulic and thermal performance of lattice structures. Contemporary literature reflects a significant focus on the empirical investigation of these structures' characteristics through advanced numerical simulations, as indicated by the substantial body of research in the field [13, 17].

This study employed a mathematical modeling approach utilizing the Ansys Fluent software package, which is based on the Navier-Stokes equations solution. The equations system was resolved using the standard model of k-ε for turbulence closure. The computational domain was discretized with a

minimum of 0.05 orthogonal quality using a hexagonal mesh comprising approximately 2.9 million cells.

The developed channel model, incorporating a lattice radiator, encompassed the computational mesh, defined the conditions of the boundary, solver parameters, and selected turbulence models. Conditions of the inlet boundary were prescribed as a mass flow rate, with static pressure, velocity, and temperature profiles specified. The inlet pressure value was derived from empirical field test data.

The pressure loss (Pa) across the lattice structure within the channel inlet is defined by the following expression:

$$\Delta P = P_{inlet} - P_{outlet} \quad (1)$$

In practical applications, hydraulic resistance is typically characterized by ξ, which is calculated using the following [14]:

$$\xi = \frac{\Delta P \cdot 2 \cdot d_n \cdot \Pi}{\rho \cdot w^2 \cdot L} \quad (2)$$

where, d_n = channel hydraulic diameter, [m] = characteristic dimensions of Nusselt and Reynolds numbers; ρ = air flow density [kg/m^3] at the entrance of the channel lattice part; Π = lattice insert porosity obtained from a ratio of (voids volume/total volume) of the porous body; w = air flow speed at the entrance of the channel lattice part, [m/s]; L = length of the lattice structure, [m].

In this study, the mathematical modelling was conducted using the Ansys Fluent package by solving the Navier–Stokes Eq. (3). The equations system was closed using k-ε turbulence standard model Eq. (4) and Eq. (5). Momentum conservation equations for an incompressible fluid were defined as:

$$\rho\left(\frac{\partial v}{\partial t} + v \cdot \nabla v\right) = -\nabla p + \mu \nabla^2 v + \rho f \quad (3)$$

where, ρ = the density of the liquid, t = time, v = velocity vector, μ = dynamic viscosity, p = pressure, f = external forces (e.g. gravity).

Kinetic energy equation of turbulence κ:

$$\rho\left(\frac{\partial v}{\partial t} + v \cdot \nabla \kappa\right) = \nabla\left(\left(\mu + \frac{\mu_t}{\sigma_\kappa}\right)\nabla \kappa\right) + P_\kappa - \rho\varepsilon \quad (4)$$

where, μ_t = turbulent viscosity (depends on κ and ε), σ_k = empirical constant, P_k = production of kinetic energy of turbulence.

The equation for the rate of energy dissipation ε:

$$\rho\left(\frac{\partial \varepsilon}{\partial t} + v \cdot \nabla \varepsilon\right) = \nabla\left(\left(\mu + \frac{\mu_t}{\sigma_\varepsilon}\right)\nabla \varepsilon\right) + C_{1\varepsilon}\frac{\varepsilon}{\kappa}P_\kappa - C_{2\varepsilon}\rho\frac{\varepsilon^2}{\kappa} \quad (5)$$

where, σ_ε = the empirical constant, $C_{1\varepsilon}$ and $C_{2\varepsilon}$= empirical constants.

2.3 Experimental work

The experiments were performed in an open-circuit wind tunnel, equipped with instrumentation for measuring static pressure, total pressure, and inlet fluid temperature. The experimental setup and its schematic are presented in Figures 2 and 3. As shown in Figure 4, the test section was rigidly fixed inside the outlet pipe using a locking bolt to guarantee immobility and accurate alignment. Unfiltered ambient air served as the working fluid, with flow velocities regulated between 5 m/s and 60 m/s. Hydraulic performance was evaluated for three different test configurations (see Figures 5-7 for their geometry and dimensions). Two of these were 50 mm long, square (20 × 20 mm) channels filled with PHEs of differing densities.

Figure 2. External view of the experimental setup used for hydraulic characterization

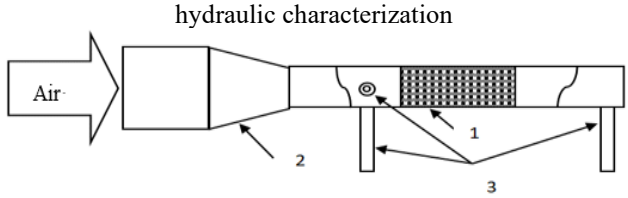

Figure 3. Schematic diagram of the working section layout
Note: 1 – installation location of the lattice element (test section), 2 – inlet confuser for flow stabilization, 3 – taps for measuring static and total pressure, air was used as the working fluid

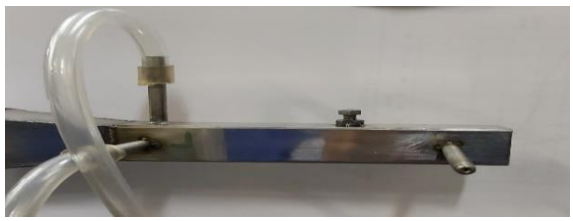

(a) longitudinal

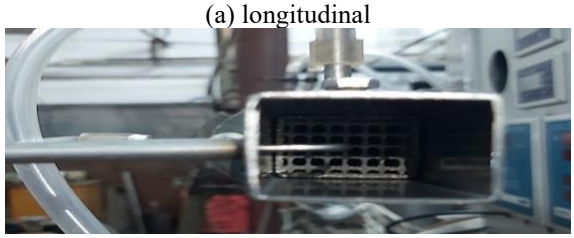

(b) cross-section

Figure 4. Appearance of the working area installed in the test section: (a) longitudinal view showing the channel; (b) cross-sectional view

Porosity degree of area No. 1 was Π = 0.0914, area No. 2, Π = 0.1096. As follows from Figure 5, the increase in the degree of porosity of the channel was carried out by increasing the layers; hence, the size of the pore decreased, but the third section still had a smooth, hollow channel (50 mm long and 20 × 20 mm in cross-section). This work area functioned as a

foundation for testing and comparison with the hydraulic properties of channels containing lattice structures.

The setup is an open-air flow circuit containing pressure and temperature measurement systems.

The section was fixed with a locking bolt to ensure immobility during testing.

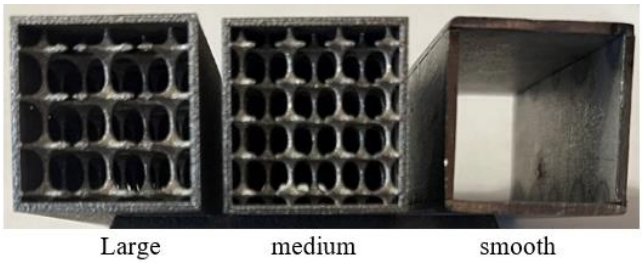

Figure 5. Appearance of working lattice sections

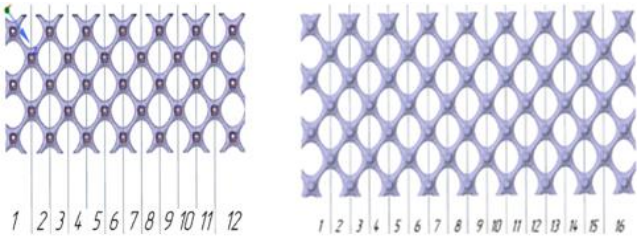

Figure 6. Scheme of a longitudinal section of working areas

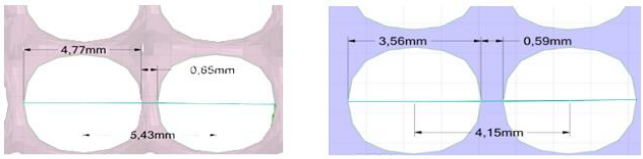

Figure 7. Geometric parameters of the pores of three working sections

2.4 Ethics statements

The authors affirm that there are no financial or personal relationships that could be construed as influencing the research presented in this work.

3. RESULTS AND DISCUSSION

3.1 Analysis of hydraulic performance

The core experimental findings quantifying the hydraulic performance of the tested channels are presented in Figures 8 and 9. As shown in Figure 8, the dependence of the pressure drop (ΔP) on the incoming flow velocity for the smooth channel and the two channels equipped with lattice structures of different densities (No. 1, Π = 0.0914; No. 2, Π = 0.109).

As anticipated, the smooth channel demonstrates a classic, relatively moderate increase in pressure drop with flow velocity, governed primarily by wall friction. In stark contrast, both lattice-filled channels exhibit a significantly steeper, non-linear growth in ΔP. This behavior is a direct manifestation of the complex fluid dynamics introduced by the lattice. The flow within these structures is characterized by repeated acceleration, deceleration, impingement on struts, and vortex shedding, which collectively transform pressure into turbulent kinetic energy, resulting in substantially higher dissipative losses [13, 15].

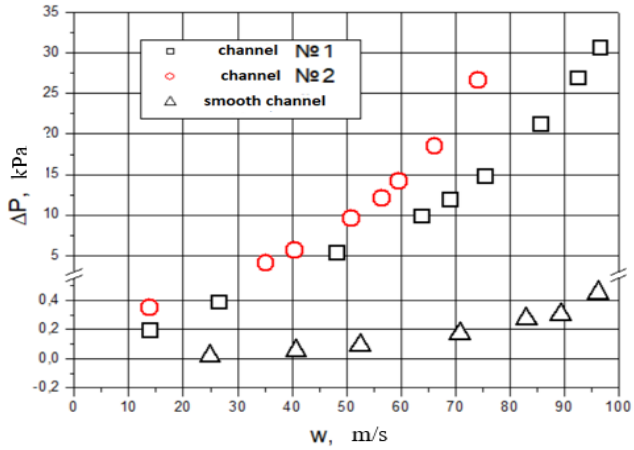

Figure 8. Measured pressure drop (ΔP) versus air velocity for smooth and lattice-filled channels (Densities No. 1 and No. 2)

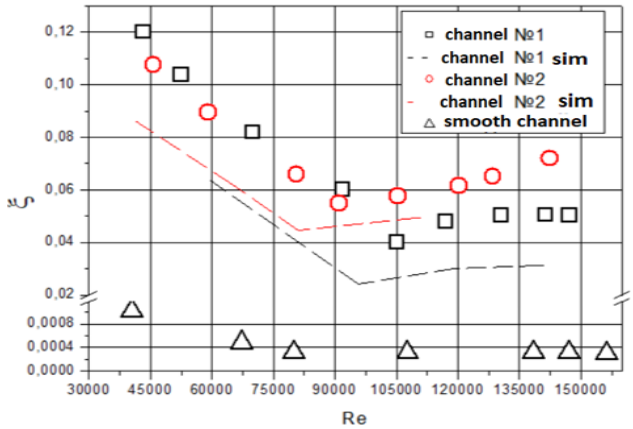

Figure 9. Hydraulic resistance coefficient (ξ) vs. Reynolds number (Re) for smooth and lattice-filled channels. Symbols: experiments; dashed lines: k-ε model simulations

A critical observation from Figure 8 is the performance stratification between the two lattice densities. While the pressure drop values for Channels No. 1 and No. 2 are close at lower velocities (below ~40 m/s), they diverge markedly at higher flow rates. Channel No. 2, with its higher density of internal elements and consequently smaller pore size, consistently generates a greater pressure drop. This is mechanistically explained by the increased flow constriction and the larger total wetted surface area in Channel No. 2, which amplifies viscous drag forces. At a flow velocity of 75 m/s, this difference becomes particularly pronounced, with ΔP for Channel No. 2 exceeding 12 kPa, compared to a lower value for Channel No. 1.

To generalize these findings and enable comparison with other systems, (ξ) is plotted against the Reynolds number (Re) in Figure 9. The data reveals that ξ decreases with increasing Re for all configurations, a trend typical for flows in rough and porous passages transitioning into a fully developed turbulent regime [14]. The convergence of the ξ curves for the two lattice structures at lower Re (Re < 90,000) suggests that the flow behavior is initially similar, likely dominated by inertial

effects at the macro-structure level. However, for Re > 90,000, the curves stratify, with Channel No. 2 exhibiting a systematically higher hydraulic resistance coefficient. This indicates that at higher flow rates, the increased geometric complexity and smaller hydraulic diameter of the denser lattice begin to dominate the flow resistance, leading to less efficient hydraulic performance compared to the sparser lattice of Channel No. 1.

The plot shows a significant and non-linear increase in pressure drop for lattice-filled channels, which escalates with lattice density at higher velocities.

The graph demonstrates the systematic underestimation of hydraulic resistance by the numerical model compared to experimental results.

3.2 Critical evaluation of numerical model against experimental data

To complement the experimental analysis and gain deeper insight into the flow fields, a numerical study was conducted using the Ansys Fluent package with k-ε turbulence standard model. The channel computational model with the lattice radiator was built using a high-quality mesh, exemplified for the medium-density lattice in Figure 10. The mesh consisted of an average of 2.9 million hexagonal cells, with careful attention paid to resolving the complex geometry of the struts, achieving a minimum of 0.05 orthogonal quality. The solving process was carried out until the residuals for energy reached a precision of 10-6, ensuring convergence.

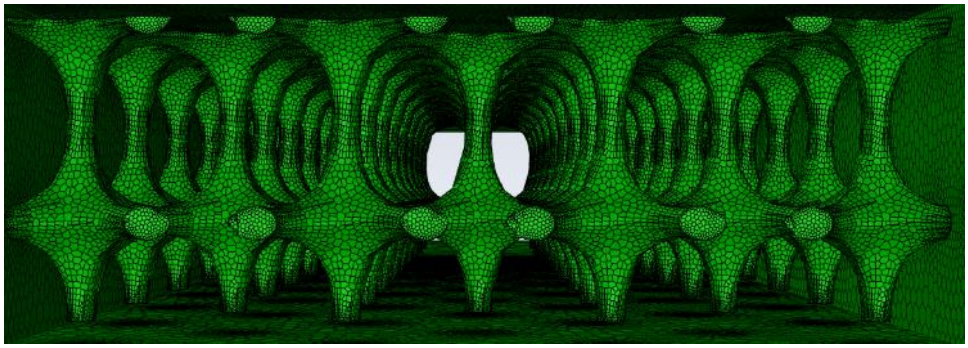

Figure 10. Computational mesh for the medium-density lattice radiator (Channel No. 2)

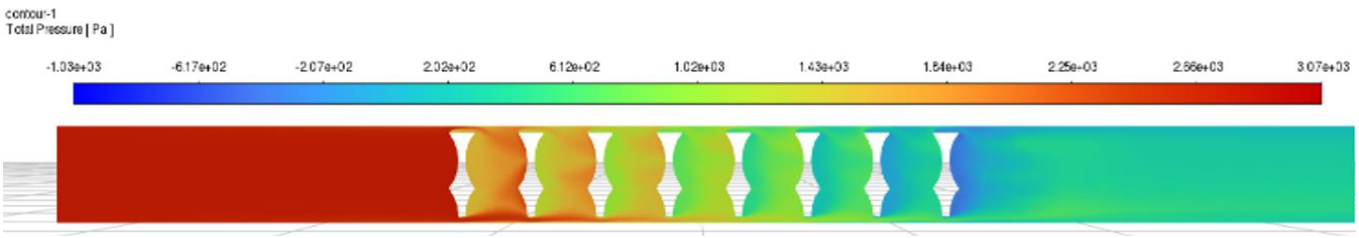

Figure 11. Contour plot of total pressure in the longitudinal section of Channel No. 2 (medium-density lattice), from simulation

An example of the resulting flow field is shown in Figure 11, which depicts the distribution of total pressure in a longitudinal section of the channel with the lattice insert. The model successfully resolves the complex flow patterns, including pressure gradients across the lattice and the wake regions behind the struts.

Qualitatively, the model successfully captures the overall trend of decreasing ξ with increasing Re for both lattice structures, which aligns with findings in similar studies of complex porous media [17]. This confirms the model's ability to predict the general scaling of hydraulic losses. However, a quantitative analysis reveals a significant and systematic discrepancy: the k-ε model consistently underestimates the hydraulic resistance across the entire range of Reynolds numbers. The magnitude of this underestimation is substantial, averaging 42% for Channel No. 1 and 25% for Channel No. 2 in the mid-range of Re.

We attribute this discrepancy primarily to the idealized representation of the lattice surface in the numerical model. The computational geometry was based on the nominal CAD model, which assumes perfectly smooth struts. This stands in stark contrast to the actual morphology of the SLM-fabricated lattices, as unequivocally revealed by the SEM micrographs in Figure 1. The significant surface roughness (Ra ≈ 20 μm), the presence of partially sintered powder particles adhering to the struts (Figures 1(b) and (c)), and the micro-scale deviations from the ideal geometry introduce additional sources of flow disturbance and viscous drag that are not captured by the k-ε model with standard wall functions [11, 17]. This model family is known to be less accurate for flows with strong separations and reattachments, which are exacerbated by surface roughness.

The finding that the discrepancy is larger for the sparser lattice (Channel No. 1) is particularly insightful. In a sparser structure, the relative contribution of form drag (from the overall shape of the struts) to the total pressure drop is high, and the model captures this reasonably well. However, the relative importance of skin friction drag (directly influenced by surface roughness) is also significant. In the denser lattice (Channel No. 2), form drag likely dominates to such an extent that the additional penalty from surface roughness constitutes a relatively smaller fraction of the total error, hence the smaller percentage discrepancy. This hypothesis aligns with the data showing a reduction in the error margin for Channel No. 2 at higher Re numbers (from 25% to 15%), where inertial forces and form drag are even more prevalent.

The mesh consists primarily of hexagonal cells, with local refinement to capture the geometry of the struts. This is an

original visualization from the present study.

The pressure drop across the lattice structure is visible in the original visualization shown above.

3.3 Implications for design and modeling

The consistent underestimation of hydraulic resistance by the standard k-ε model has critical implications for lattice-based heat exchangers' design. Relying solely on such simulations would lead to overly optimistic predictions of pumping power requirements, potentially resulting in underperforming thermal management systems.

Therefore, for accurate predictive modeling, two paths can be pursued. First, the surface roughness can be explicitly incorporated into more advanced turbulence models, such as the Transition SST or Large Eddy Simulation (LES), though at a greatly increased computational cost [17]. Second, a practical engineering approach involves calibrating the porous media models or correlation-based models using experimental data from representative SLM-fabricated samples, effectively "baking in" the roughness effect through empirically derived coefficients.

The results presented here, while focused on hydraulics, underscore the dual nature of SLM-fabricated lattice structures. Their immense surface area is a clear asset for heat transfer intensification [5, 7]. However, this very surface, with its inherent roughness, is also a primary source of hydraulic loss. This highlights the fundamental trade-off that designers must navigate: the gain in thermal performance versus the penalty in pumping power. Optimizing lattice structures for thermal-hydraulic efficiency will thus require a multi-objective approach that explicitly accounts for the as-built surface morphology from the SLM process.

4. CONCLUSION

This study experimentally and numerically characterized the hydraulic performance of channels integrated with SLM-fabricated spatial lattice structures of varying densities. The main conclusions are:

•Spatially ordered lattice structures induce a significantly higher pressure drop compared to smooth channels, which increases with lattice density due to greater flow constriction and surface area.

•The standard k-ε turbulence model, while capturing qualitative trends, systematically underestimates the hydraulic resistance. This is primarily attributed to its inability to account for the significant surface roughness and micro-scale morphological imperfections inherent to the SLM process, as evidenced by micrographic analysis.

•Despite the increased hydraulic resistance, the immense surface area offered by lattice structures makes them potent candidates for high-flux compact heat exchangers where thermal performance is prioritized, and the pressure penalty can be managed.

Limitations and future work:

A key limitation of this study is the use of an idealized numerical model that does not incorporate surface roughness. This work was also focused on hydraulic performance; concomitant thermal measurements are essential for a complete thermal-hydraulic assessment.

Future research should focus on: (i) quantifying the surface roughness and incorporating it into more advanced turbulence models (e.g., LES or Transition SST) or using porous media approximations with experimentally calibrated coefficients; (ii) conducting conjugate heat transfer analysis to evaluate the overall thermal-hydraulic efficiency; and (iii) exploring multi-objective optimization of lattice unit cells to minimize pressure drop while maximizing heat transfer.

REFERENCES

[1] Sarabhai, S., Letov, N., Kibsey, M., Sanchez, F., Zhao, Y.F. (2023). Understanding the flow and thermal characteristics of non-stochastic strut-based and surface-based lattice structures. Materials & Design, 227: 111787. https://doi.org/10.1016/j.matdes.2023.111787

[2] Xue, Z., Wang, P., Yue, Z., Lian, C., Zhang, T., Gao, M. (2024). Advanced cooling channel structures for enhanced heat dissipation in aerospace. Applied Thermal Engineering, 248: 123346. https://doi.org/10.1016/j.applthermaleng.2024.123346

[3] Bajaj, P., Hariharan, A., Kini, A., Kürnsteiner, P., Raabe, D., Jägle, E.A. (2020). Steels in additive manufacturing: A review of their microstructure and properties. Materials Science and Engineering: A, 772: 138633. https://doi.org/10.1016/j.msea.2019.138633

[4] Leary, M., Mazur, M., Williams, H., Yang, E., et al. (2018). Inconel 625 lattice structures manufactured by Selective Laser Melting (SLM): Mechanical properties, deformation and failure modes. Materials & Design, 157: 179-199. https://doi.org/10.1016/j.matdes.2018.06.010

[5] Sunil, A.K., Kumar, R. (2021). Designing a more effective finned automotive radiator cooling process using carbon nanotube-water nanofluid turbulent flow. Suranaree Journal of Science & Technology, 28(4): 010056.

[6] Hu, C., Sun, M., Xie, Z., Yang, L., Song, Y., Tang, D., Zhao, J. (2020). Numerical simulation on the forced convection heat transfer of porous medium for turbine engine heat exchanger applications. Applied Thermal Engineering, 180: 115845. https://doi.org/10.1016/j.applthermaleng.2020.115845

[7] Liu, X., Huang, Y., Wang, C.H., Zhu, K. (2020). Solving steady and transient radiative transfer problems with strong inhomogeneity via a lattice Boltzmann method. International Journal of Heat and Mass Transfer, 155: 119714. https://doi.org/10.1016/j.ijheatmasstransfer.2020.119714

[8] Hamidi, E., Ganesan, P., Muniandy, S.V., Amir Hassan, M.H. (2022). Lattice Boltzmann method simulation of flow and forced convective heat transfer on 3D micro X-ray tomography of metal foam heat sink. International Journal of Thermal Sciences, 172: 107240. https://doi.org/10.1016/j.ijthermalsci.2021.107240

[9] Yun, S., Kwon, J., Cho, W., Lee, D., Kim, Y. (2020). Performance improvement of hot stamping die for patchwork blank using mixed cooling channel designs with straight and conformal channels. Applied Thermal Engineering, 165: 114562. https://doi.org/10.1016/j.applthermaleng.2019.114562

[10] Ryazhskih, V.I., Konovalov, D.A., Nikolenko, A.V. (2018). Heat transfer model analysis of a hybrid porous compact heat exchanger. In 2018 International Multi-Conference on Industrial Engineering and Modern

Technologies (FarEastCon), Vladivostok, Russia, pp. 1-6. https://doi.org/10.1109/FarEastCon.2018.8602905

[11] Xiao, Z., Yang, Y., Xiao, R., Bai, Y., Song, C., Wang, D. (2018). Evaluation of topology-optimized lattice structures manufactured via Selective Laser Melting. Materials & Design, 143: 27-37. https://doi.org/10.1016/j.matdes.2018.01.023

[12] Sing, S.L., Wiria, F.E., Yeong, W.Y. (2018). Selective Laser Melting of lattice structures: A statistical approach to manufacturability and mechanical behavior. Robotics and Computer-Integrated Manufacturing, 49: 170-180. https://doi.org/10.1016/j.rcim.2017.06.006

[13] Wang, X., Chen, M., Tate, D., Rahimi, H., Zhang, S. (2020). Numerical investigation on hydraulic and thermal characteristics of micro latticed pin fin in the heat sink. International Journal of Heat and Mass Transfer, 149: 119157. https://doi.org/10.1016/j.ijheatmasstransfer.2019.119157

[14] Popov, I.A., Shchelchkov, A.V., Skrypnik, A.N., Ryzhkov, D.V., Zubkov, N.N., Zhukova, Yu V., Sverchkov, S.A. (2018). Hydraulic resistance of tubes with internal helical finning designed by deforming cutting. Journal of Physics: Conference Series, 980: 012004. https://doi.org/10.1088/1742-6596/980/1/012004

[15] Saghir, M.Z., Kerme, E.D., Hajialibabei, M., Rasheed, H., Welsford, C., Al-Ketan, O. (2024). Study of the thermal and hydraulic performance of porous block versus gyroid structure: Experimental and numerical approaches. Energies, 17(4): 861. https://doi.org/10.3390/en17040861

[16] Kuang, X., Sansalone, J., Ying, G., Ranieri, V. (2011). Pore-structure models of hydraulic conductivity for permeable pavement. Journal of Hydrology, 399(3-4): 148-157. https://doi.org/10.1016/j.jhydrol.2010.11.024

[17] Jiang, Z., Deng, T., Yin, Q., He, L. (2021). Numerical modeling of fluid flowing properties through porous media with single rough fractures. Geofluids, 2021: 1-21. https://doi.org/10.1155/2021/6611723

[18] Lopatin, A.A., Gabdullina, R.A., Biktagirova, A.R., Terentyev A.A. (2023). Heat transfer of a radiator with a spatial lattice ordered structure under conditions of free convection. Journal of International Academy of Refrigeration, (4): 33-43. https://doi.org/10.17586/1606-4313-2023-22-4-33-4

[19] Lopatin, A.A., Gabdullina, R.A., Saetgaraev, A.A, Kurshev, E.D. (2025). Hydraulic characteristics of spatially lattice channels in cooling systems of heat-loaded elements of airborne radio-electronic equipment. Russian Aeronautics, 68(1): 1-9. https://doi.org/10.3103/S1068799825010015

[20] Liu, F., Mao, Z., Zhang, P., Zhang, D.Z., Jiang, J., Ma, Z. (2018). Functionally graded porous scaffolds in multiple patterns: New design method, physical and mechanical properties. Materials & Design, 160: 849-860. https://doi.org/10.1016/j.matdes.2018.09.053

[21] EOS GmbH (Electro Optical Systems). (n.d.). EOS StainlessSteel PH1 material data sheet. https://www.eos.info/metal-solutions/data-sheets/all-processes-and-materials?id=eos-stainlesssteel-ph1&topdf=/metal-solutions/data-sheets/all-processes-and-materials?id=eos-stainlesssteel-ph1&pdf=1.